J Mol Model (2004) 10:112–120
DOI 10.1007/s00894-004-0181-1

ORIGINAL PAPER

Wei Zhang · Ting-Jun Hou · Xue Bin Qiao · Sun Huai · Xiao Jie Xu

Binding affinity of hydroxamate inhibitors of matrix metalloproteinase-2

Received: 30 June 2003 / Accepted: 24 November 2003 / Published online: 21 February 2004
© Springer-Verlag 2004

Abstract Here we report molecular dynamics (MD) and free energy perturbation (FEP) simulations applied to hydroxamate-matrix metalloproteinase-2 (MMP-2) complex systems. We have developed some new force field parameters for the hydroxamate functional group that were not included in the AMBER94 force field but were necessary in our simulations. For the representation of the active zinc center, a bonded model was adopted in which restrained electrostatic potential fitting (RESP) charges were used as the electrostatic representation of this model. Using the resulted bonded model, FEP simulations predict the relative binding free energy in good agreement with the experimental value. By analyzing the molecular dynamics (MD) trajectories of the two complex systems, we can provide an explanation of why one of the two inhibitors is favored over the other. The results provide a chemical insight into the interactions between inhibitor and enzyme, and can indicate changes in the inhibitor that would enhance inhibitor–enzyme interactions.

Keywords MMP-2 · Gelatinase-A · Hydroxamate · FEP · AMBER force field

Introduction

Matrix metalloproteinases (MMPs) are a large family of zinc-containing enzymes that show proteolytic activities against most components of the extracelluar matrix, such as fibronectin, laminin and interstitial collagens. [1, 2, 3] This activity is controlled by what are known as endogenous tissue inhibitors of metalloproteinases (TIMPs) and nonspecific a2-macroglobulins. [1, 2, 3] MMPs are important therapeutic targets for treatment of many diseases involved in tissue turnover and maintenance such as cancer, arthritis, joint destruction and Alzheimer's disease, and have led to a considerable interest in non-peptidic inhibitors for oral administration. [4, 5, 6] In the MMP family, there are two type IV collagenases which are now termed gelatinase A (MMP-2) and gelatinase B (MMP-9) and have been described as being able to degrade type IV collagen of basal laminae as well as other nonhelical collagen domains and proteins such as fibronectin and lamnin. [7, 8]

The structures of MMP-2 can be divided into four subdomains: the signal peptide domain, the propeptide domain, the catalytic domain and the hemopexin-like domain. There are two zinc atoms in the catalytic domain of MMP-2. One plays a catalytic and the other a structural role. [9] The catalytic zinc atom coordinates with three histidine residues contained within the conserved –VAA-HEXGHXXGXXH– sequence of the catalytic domain and a cysteine in another conserved sequence –PRCGXPD– of the propeptide amino-terminal domain. The interaction with cysteine must be broken before the metalloproteinase can degrade extracelluar matrix. According to the X-ray structures of MMPs and some other information, a generalized catalytic mechanism has been generated, [10] as illustrated in Fig. 1. Firstly, the peptide is coordinated to the catalytic zinc ion via a zinc–carbonyl interaction. Then a water molecule transfers a proton to Glu-202, and this glutamic acid transfers its proton to the amide nitrogen of the peptide, which facilitates the degradation of the starting protein into two peptide fragments. Finally, the peptide fragments are lost to generate the resting state on the enzyme. Numerous questions remain regarding this catalytic mechanism, but this is a working mechanism until further corroborating data is obtained.

Many effective inhibitors on MMPs have been reported during the last decade, and it has been revealed that all these inhibitors are similar in many aspects. They all have a zinc-binding group (ZBG) on one end that plays a very

W. Zhang · T.-J. Hou · X. B. Qiao · X. J. Xu (✉)
College of Chemistry and Molecular Engineering,
Peking University,
100871 Beijing, People's Republic of China
e-mail: xiaojxu@chem.pku.edu.cn
Tel.: +86-10-62757456
Fax: +86-10-62758076

S. Huai
Aeon Inc., USA

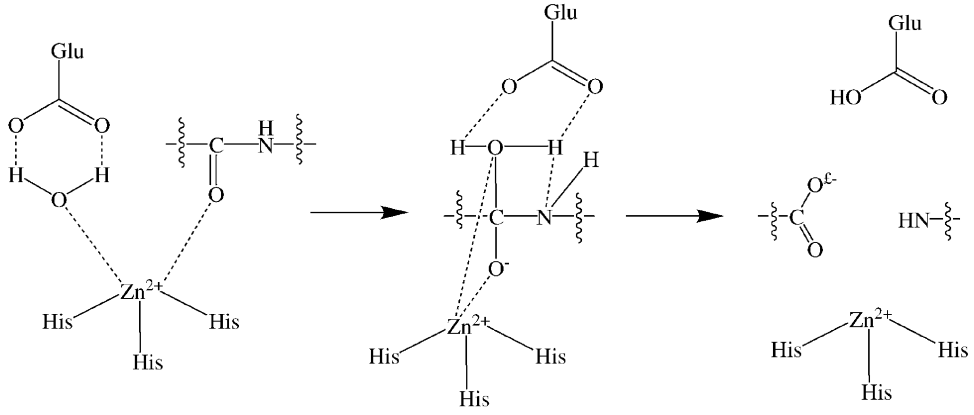

Fig. 1 The catalytic mechanism of MMP

important role in the interaction energy between the inhibitor and the protein. Inhibitors with many types of zinc-binding groups, such as hydroxamate, carboxylate, aminocarboxylate, and sulfydryl have been synthesized and tested. Among all these inhibitors, inhibitors with a hydroxamate zinc-binding group have been found to be the most potent. Another important component of a good inhibitor of MMPs is a long, large and nonpolar functional group attached to the zinc-binding group called the P1' substituent, which can make good van der Waals interaction with the S1 pocket of the enzyme. [1]

Crystal structures of many MMP–hydroxamate complexes have been determined using X-ray diffraction, from which we can get a clear picture of the interaction mechanism between hydroxamates and MMPs. These crystal structures have shown that the catalytic zinc ion is chelated by the two oxygen atoms on the hydroxamate, and is in total pentacoordinated. [11, 12]

To model the catalytic domain of MMPs using a potential function method, we should select a way in which to represent the coordinate interaction between the catalytic zinc ion and its ligands (three histidines and one hydroxamate). There are basically two ways to parameterize the coordinate interaction: the bonded model [13, 14, 15, 16, 17, 18] and the nonbonded model; [19, 20, 21, 22, 23] neither is entirely satisfactory. Recently, Donini and Kollman reported their simulation of MMP-3 using a nonbonded approach and AMBER force field, but they also failed in reproducing the binding geometry of the complex and could not predict the rank of binding free energy correctly. [11] Thus, given our past success with the bonded model, we decided to continue its use in the current work. [15, 16, 17, 18]

Here we report MD and free energy perturbation (FEP) simulations applied to two hydroxamate inhibitors bound to the catalytic domain of matrix metalloproteinase-2 (MMP-2). We had developed some force field parameters for the hydroxamate functional group which were not included in AMBER parm94 but were necessary in our simulations. A bonded model was adopted to represent the active zinc center, and restrained electrostatic potential fitting (RESP) charges were used to represent the electrostatic representation of this model. Secondly, the binding preference of the two ligands was investigated by using MD and FEP simulations. We expect that based on the result of FEP, we can provide a reasonable explanation why inhibitor B is favored over inhibitor A. Moreover, from the analysis of the MD trajectories, we expect to gain insight into the structure requirement of hydroxamate bound to MMP-2 and give some useful information for the structure modification.

Methodology

Starting conformation

Before this work was performed several crystal structures of MMP-2s had been determined and are now available in the Protein Data Bank, but none of them has a hydroxamate inhibitor bound to its active site. So we encountered a problem about how to get a correct complex structure for our simulations. We chose to use the structure of an MMP-3–hydroxamate complex as reference to build the structure of the MMP-2–hydroxamate complex. We chose MMP-3 as reference protein because MMP-3 is very similar to MMP-2, both in sequence and structure. The sequence similarity between the two sequences is 60.08%, and the RMSD between the active sites of the two structures is only 0.71 Å. (Here we define active site to include three histidines that coordinate to the catalytic zinc ion His-201,His-205, His-211 and the S1 pocket which consists of Val-197, Ala-198, Glu-202, Ile-218 and Tyr-223, but Ile-218 cannot be superimposed because it has mutated into leucine in MMP-3, so in total six residues were superimposed.) For the structure of MMP-2 we used the crystal structure determined by Dhanaraj et al. (PDB entry 1qib); [24] for the structure of MMP-3-hydroxamate complex with a hydroxamate inhibitor we used the structure determined by Chen et al.(PDB entry 1b3d). [25]

The conformation was built using the following procedure. Firstly, we fitted the two structures' enzyme parts together by structural alignment; then we extracted inhibitor S27 from 1b3d and merged it into 1qib.Finally, we modified the structure of S27 to meet with the structures of inhibitor A and inhibitor B, respectively (the structures of inhibitor A and inhibitor B are shown in Fig. 2). During the model-building process, the conformation of the protein was not altered, and the structures of inhibitors were altered minimally to avoid unacceptable atom bumps. We placed five bonds between the zinc ion and His-201, His-205, His-211 and the two oxygen atoms of the hydroxamate's zinc binding group. This was done using the InsightII molecular simulation package. [26]

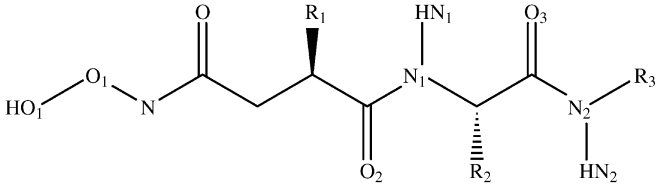

A: R_1=-$(CH_2)_3C_6H_{11}$ R_2= -$CH_2C_6H_{11}$ R_3= -$(CH_2)_2C_6H_5$

B: R_1=-$(CH_2)_3C_6H_5$ R_2= -$CH_2C_6H_{11}$ R_3= -$(CH_2)_2C_6H_5$

Fig. 2 The studied inhibitors

Force field

To model the hydroxamate functional group using a classical potential function such as AMBER, force field parameters associated with the N–O functionality must be developed since these are not available in the current AMBER94 force field. We took acetohydroxamate ($CH_3C(O)NHOH$) as the small molecular model system of the hydroxamate functional group. The structure was optimized using an ab initio computation at the HF/6-31G* MP2 level. Then we performed a single-point energy computation and normal-mode coordinate analysis on the optimized structure to obtain its Hessian matrix. Only by fitting it can we derive the force field parameters. The derived force field parameters are listed in Table 1. The ab initio computation was done using Gaussian 98, [27] and the force field fitting was done using the Direct Force Field 1.0, software newly developed by Dr. Sun Huai in Aeon Inc. [28]

The bond and angle parameters associated with the zinc center were taken from Hoops et al. All the torsions associated with the zinc–ligand bonds were set to the default values as in Hoops et al. [13]

Partial charges

Together with the derived force field parameters, we should develop an appropriate electrostatic representation of the MMP's active site. It has been reported that a nonbonded metal–ligand representation involving a formal charge (+2) often leads to octahedral coordination for zinc, [13] so we adopted and extended the bonded model approach with partial charges. Here restrained electrostatic potential fitting (RESP) charges were used instead of ESP charges, because RESP charges can reduce the excessive polarity often exhibited with ESP charges. [29] We include the catalytic zinc ion, the side chains of three histidines and the inhibitor's hydroxamate functional group in the active site. It was optimized at first using a semiempirical QM calculation with the PM3 Hamiltonian. Then ab initio computation at the HF/6-31G* level was used on the optimized structure to obtain the electrostatic potentials, which can be used for deriving partial charges. The two inhibitors used in this research should be built and optimized for the computations of the electrostatic potentials, just as was done for the active site. Only by finishing these all, can we begin the fitting procedure for our desired electrostatic representation. The work was done using the Cerius2 molecular modeling package. [30]

The fitting procedure can be divided into two stages: one for the active site, and the other for the two inhibitors. Firstly, we got the partial charges of the atoms included in the active site using RESP. Then, we got the partial charges of the inhibitor by fitting the electrostatic potentials with the charge of atoms in the zinc binding group constrained to the particle charges determined in the first stage. The derived RESP charges are provided as supporting information in AMBER format.

Table 1 The force-field parameters for the catalytic zinc ions and hydroxamates

Bond	Kr (kcal mol^{-1} Å^{-2})	Req (Å)	
Zn–NB	40.0	2.05	
Zn–OH	40.0	2.20	
Zn–O	40.0	2.05	
N–O	450.3	1.35	
Angle	Kθ (kcal mol^{-1} rad^{-2})	θeq (°)	
NB–Zn–NB	20.0	105.0	
NB–Zn–O	20.0	115.0	
CR–Zn–NB	20.0	126.0	
N–OH–HO	52.6	100.6	
OH–N–C	83.4	109.2	
H–N–OH	66.0	100.8	
Dihedral	v (kcal mol^{-1})	γ (°)	N
HO–OH–N–C	0.0194	0	6
HO–OH–N–H	–0.6123	0	6
O–C–N–OH	–5.2643	0	2
CT–C–N–OH	–0.4905	0	2

The structures of inhibitors were built and optimized using MOPAC 7.0. [31] The ab initio calculations were performed using Gaussian 98, and the RESP charges were generated using the *resp* module of AMBER 6.0. [29]

The partial charges for the inhibitors in aqueous-solvent environment were determined using the RESP charges with no constraints applied. The electrostatic potentials used for fitting were determined in the gas phase, and this may lead to a systematic error, but what we need in the final is the dispersion of free energy of the two inhibitor, and the two compounds are so similar that the systematic error might be counteracted in our simulations.

From the calculations we can see the partial charges on three histidines coordinated with the catalytic zinc ion are quite different, and they are also significantly different from the standard AMBER values, so we need to make some modifications to the AMBER database file and PDB file to recognize these three different residues properly. In AMBER, we defined thee kinds of new residue: HIA, HIB and HIC, and they represented His-201, His-205 and His-211 in 1qib, respectively. The partial charges on these three newly defined residues were revised from the default values in AMBER to the ESP charges in this paper. The derived partial charge on the zinc ion is 0.85|el, while Toba et al. used a value of 0.80|el in their simulation of MMP-3 using a bonded model. Moreover, we defined a new zinc unit to represent the catalytic zinc center. Each ligand studied was defined as a new type of residue and added to the AMBER database files. All newly developed force field parameters in Table 1 were added to the AMBER force field file.

Minimization and MD simulations

This part of the work was done on two kinds of system: the complex and the inhibitor. It should be noted that all the systems were solvated in a water cap filled up to 20 Å. For the complex, the solvated cap was around the catalytic zinc ion, and for the inhibitor it was around the inhibitor's geometrical center. Two sodium ions were added to the complex system to keep the system's total charge zero. The preparing work was finished using *xleap*, a graphical interface provided by AMBER 6.0.

Before the MD simulations, we optimized the protein structure to validate the derived force field parameters and the electrostatic representation. After a 5,000-step minimization (steepest descent for the first 500 steps, and conjugate gradient for the rest) with a 16-Å atom-based nonbonded cutoff, we obtained a structure in good agreement with the X-ray structure with an RMS derivation of only 0.17 Å. MD trajectories were then obtained using the optimized structure as the starting conformation. In the whole MD simula-

tions, for the two complexes a harmonic potential constraint of 15.0 kcal mol^{-1} $Å^{-2}$ was applied on residues whose distance to the catalytic zinc ion was more than 15 Å. All the simulations included a SHAKE constraint on all covalent bonds involving hydrogen; a time step of 1.5 fs and a nonbonded cutoff of 12 Å were used. MD simulations were run at 300 K and the system was warmed from 0 K to 300 K over 50 ps followed by a 1,000-ps MD simulation. The conformations were recorded as snapshots every 20 ps, five of them were later used as the starting points for the FEP simulations, the rest was used for the analysis of the enzyme–inhibitor interaction energy.

Free energy perturbation

FEP simulations were carried out using the *gibbs* module of the AMBER 6.0. [32] Both the "fixed width window growth" and "slow growth" approaches were employed on the complex system, while only the "fixed width window growth" method was employed on the inhibitor system in determining the relative binding free energy. The "slow growth" method was employed because it can give the exact contribution of each energy term in the force field potential function, and this information may be very useful for our further discussions. The mutation present here was the perturbation from a cyclohexene ring to a benzene ring, in which six hydrogen atoms disappeared and six carbons were mutated from CT(sp^3) to CA(sp^2).

For the "fixed width window growth" method we set the window number to 21 and for each window an 30 ps equilibration period follow by a 20-ps period for data collection. For the "slow growth" method total 1,000-ps simulations were performed to complete the perturbation. For the complex system, complete motional freedom was given to the ligand and the residues within 10-Å distance around the catalytic zinc atom, other atoms were fixed. For the inhibitor system, complete motional freedom was given to the inhibitor and the water molecules within 10-Å distance around the geometrical center of the inhibitor. Other parameters were the same as those in the above MD simulations except SHAKE constraints were not used because the mutation involved hydrogen atoms.

Results and discussion

First of all, we must check that we have reproduced the active site and the binding geometry successfully because distortion of the binding site might affect the accuracy of the computed free energies. The hydroxamate zinc-binding group acts as a chelate ligand with each oxygen (O and O1) coordinated to the active-site zinc ion at an optimum distance, usually 1.9–2.3 Å. In our simulations, the binding geometry is retained well. We have measured the average distance between the catalytic zinc ion and the five coordinated atoms in the MD procedure, and found they are in good agreement with distances determined crystallographically. All the distances are shown in Tables 2, 3 and 4, and the standard deviations of the average distance are also included for reference. This agreement is not very surprising because of the bonded model we have used to represent the system.

The degree to which the hydrogen bonds between the inhibitor and the protein are reproduced is another important criterion for the accuracy of the simulated complex. It has been reported that hydrophilic interactions such as hydrogen bonds between the inhibitor-amide protons and the enzyme were extremely important in stabilizing the inhibitor in the active site. [33] From the X-ray structure of MMP-3–hydroxamate complex, we found that several strong hydrogen bonds are formed between the enzyme and the inhibitor. Because of the high structure similarity between the active site of MMP-2 and that of MMP-3(RMSD 0.71 Å), these hydrogen bonds should be maintained in our MD simulations. The MD data were analyzed for the complexes involving inhibitor A and inhibitor B. Both inhibitor A and inhibitor B form approximately 5–6 stable hydrogen bonds with the protein. The distances and angles of the available hydrogen bonds are given in Tables 2, 3 and 4, and the corresponding distances and angles determined crystallographically for the MMP-3–hydroxamate complex are also included for comparison. In addition to the distances of the hydrogen bonds, the standard deviations provide some indication of their strength, with derivations of about 0.1 Å characterizing a strong interaction. Among the five hydrogen bonds, the one between OE1 of Glu-202 and O1 of the inhibitor is of great importance. As we know, Glu-202 plays an important role in the proteolytic activity of the enzyme. By forming this hydrogen bond, hydroxamate can restrain the proton transfer from water molecule to Glu-202, and in consequence inhibit the catalytic activity of the enzyme.

Table 2 Average zinc–ligand distances calculated from MD trajectory

Coordinator	Complex A (Å)	Complex B(Å)	X-ray (Å)
NE2 His-201	1.97(0.09)	2.10(0.07)	2.00
NE2 His-205	2.15(0.08)	2.10(0.07)	2.13
NE2 His-211	1.97(0.03)	2.02(0.07)	2.07
O Inhibitor	2.07(0.06)	2.09(0.08)	2.08
O1 Inhibitor	2.17(0.08)	2.13(0.08)	2.17

Table 3 Average inhibitor–protein hydrogen bond distances calculated from MD trajectory

	Complex A(Å)	Complex B(Å)	X-ray (Å)
O1–OE1 Glu-202	2.63(0.18)	2.56(0.08)	2.50
O2–N Leu-164	3.12(0.17)	3.07(0.14)	2.80
N2–O Pro-221	2.88(0.08)	2.89(0.10)	3.10
O4–N Tyr-223	2.93(0.17)	3.00(0.17)	2.84
N4–O Gly-162	2.92(0.13)	2.95(0.10)	2.80

Table 4 Average inhibitor–protein hydrogen bond angles calculated from MD trajectory

	Complex A(°)	Complex B(°)
O1–HO1–OE1 Glu-202	165.0(10.8)	164.9(4.2)
O2–H Leu-164–N Leu-164	163.0(11.2)	160.5(10.9)
N1–HN1–O Pro-221	163.7(4.2)	165.6(7.7)
O3–H Tyr-223–N Tyr-223	161.5(8.9)	164.0(8.7)
N2–HN2–O Gly-162	158.4(6.1)	158.3(11.2)

Table 5 Results obtained from the FEP simulations for A to B

Starting structure	$\Delta G_{complex}$ (kcal mol^{-1})		$\Delta G_{inhibitor}$ (kcal mol^{-1})		$\Delta\Delta G_{bind}$ (kcal mol^{-1})
	Forward	Reverse	Forward	Reverse	
250 ps	2.2	−2.6			
400 ps	2.4	−2.8	−0.3	0.3	
600 ps	2.4	−2.8	−0.5	0.4	
800 ps	2.3		−0.6	0.3	
1,000 ps	2.4		−0.6	0.4	
Averages	2.3±0.1	−2.6±0.2	−0.5±0.1	0.4±0.1	2.9[a]

[a] Experimental value: 2.8 kcal mol^{-1}

Table 6 Energy components of the free energy

	ΔG (800 ps) (kcal mol^{-1})	ΔG (1,000 ps) (kcal mol^{-1})
Bond+angle+dihedral	0.000	0.000
Electrostatic	1.843	1.629
VDW	−1.459	−1.120
1–4 electrostatic	1.958	1.960
1–4 nonbond	0.000	0.000
Total	2.342	2.409

Table 7 The average internal interaction energy of the system's two enzymes

	Bond+angle+dihedral (kcal mol^{-1})	VDW (kcal mol^{-1})	Electrostatic (kcal mol^{-1})
Enzyme A	94.79(10.99)	15.15(2.31)	−33.90(1.75)
Enzyme B	99.99(6.43)	14.86(1.98)	−33.13(1.78)

Binding free energies

The FEP simulations were performed on inhibitors A and B with and without (i.e., in water) the protein MMP-2. The calculations were running from A to B only starting from the equilibrated structures of the enzyme–inhibitor complex. All runs were performed five times in the forward direction to obtain insight into the statistical errors present in the calculations. For the complex system, in the first three simulations the "fixed width window growth" approach was employed and "slow growth" approach was used for the other two FEP simulations. The resulting relative free energies are listed in Table 5. For the "slow growth" method, the free energies obtained in the two directions are almost the same, and therefore only one value is listed for the last two runs of complex system. The calculated average relative binding free energy is 2.9 kcal mol^{-1}, in agreement with the experimental value of 2.8 kcal mol^{-1}. We give the following explanation for the great accuracy: there exists a very strong interaction between the inhibitor and the enzyme in the bonded model used in our simulations. This interaction is so strong that it limits the conformation space that FEP and MD can sample to a very small region. Fortunately, this region happens to be near the lowest energy conformation, which is why we predicted the relative binding free energy so well.

When we use the "slow growth" method in FEP simulations, we know how much each energy term in the potential function contributes to the total free energy, this information is illustrated in Table 6. From this information, we can deduce that: (1) bond, angle, torsion interactions make little contribution to the free energy. That is not surprising, in most occurrences, nonbonded interactions are the most important part in the interaction between the inhibitor and the enzyme. (2) In the nonbonded interactions, electrostatic interactions including normal and 1–4 interactions of these two systems contribute to the free energy positively. (3) Van der Waals (VDW) interactions of these two systems contributing to binding free energies are negative, which means that inhibitor A is more favored over B in the VDW interactions.

Firstly, we must ensure that the enzyme–inhibitor interaction energy is more important than the enzyme's internal interaction energy, otherwise the following discussion is invalid. We have calculated the internal interaction energy of the enzyme in these two systems. The results are listed in Table 7. Though the interaction en- ergies of the two enzymes can be different by as much as 3–5 kcal mol^{-1}, the standard deviation of this energy is also 3–5 kcal mol^{-1}. This indicates that there is essentially no difference in the interaction mechanism between the enzyme parts of the two complex systems. Later we will discuss the similarity of the enzyme parts of the two complex systems again, based on a structural alignment method.

Next, we calculated the nonbonded interaction between the inhibitor and the enzyme. The results were listed in Table 8. The energies are reported in two parts: the VDW interaction energy and the electrostatic interaction energy. It should be noted that both the VDW interaction energy and the electrostatic energy are the sum of the normal interaction energy and the 1–4 interaction energy, and this

Table 8 The average interaction energy between the inhibitor and the enzyme

Nonbond	VDW (kcal mol^{-1})	Electrostatic (kcal mol^{-1})
A	−59.2(3.01)	−65.0(4.51)
B	−59.4(2.97)	−77.7(4.27)
Difference	−0.2	−12.7

Table 9 The average interaction energy between the inhibitor and the environment

Nonbond	VDW (kcal mol^{-1})	Electrostatic (kcal mol^{-1})
A	−78.53(3.95)	−82.42(5.04)
B	−73.82(3.55)	−90.44(5.25)
Difference	4.71	−8.02

is very important for our following discussions. It is obvious that the electrostatic interaction energy between inhibitor B and MMP-2 is much lower than that between inhibitor A and MMP-2. This observation is consistent with the FEP results that the electrostatic interaction plays a positive role in the total free energy.

VDW interaction

The difference in the VDW interaction energy between the two systems is −0.2 kcal mol^{-1}, which is not as positive as expected because the complex's solvation free energy was not taken into consideration. We calculated the interaction energy of the inhibitor with the environment, where the environment means the enzyme and the solute. The results are listed in Table 9. Thus, we can see that the VDW energy increases from inhibitor A to B, indicating that inhibitor A is more favorable than B in the VDW interaction with the environment.

Given that the protein's structure is almost the same, the difference between the structures of the two inhibitors is the main reason for the difference in their van der Waals interaction. As is well known, the relationship between the VDW interaction energy and the solvent-accessible molecular surface is well accepted. We have calculated the solvent accessible surface area (SASA) of the two inhibitors. Inhibitor A's SASA is 243.2 Å^2, and inhibitor B's 284.2 Å^2. Their SASAs differ by only 41 Å^2, this difference cannot explain the difference in their van der Waals interactions. As we know, the enzyme's S1 pocket consists of Val-197, Ala-198, Ile-218 and Tyr-223. Among then, Val-197, Ala-198 and Ile-218 are typical nonpolar residues, so that an aliphatic P1' substituent can make stronger van der Waals interactions than aromatic P1' substituents can. This is why inhibitor A makes more van der Waals interaction than inhibitor B.

Electrostatic interaction

To gain more knowledge about the MMP–hydroxamate electrostatic interaction, we calculated the electrostatic interaction energy between the inhibitor and each residue in the enzyme (a total of 161 residues). By comparing the result we found that for most residues, the electrostatic interaction energy did not change much between the two complex systems. In fact, there are only three residues whose electrostatic interaction changes drastically (>1.0 kcal mol^{-1}). They are Asp-161, Glu-202 and His-205. Among them, Glu-202 is known as a special residue that can play a key role in the catalytic reaction and can form a strong hydrogen bond with the inhibitor. His-205 is one of the three histidines coordinated to the catalytic zinc ion. The interaction energy between the inhibitor and the three residues for the two complex systems are listed in Table 10. The sum of the three residues' energy difference is −12.2 kcal mol^{-1}, while the total electrostatic interaction difference between the two systems is −12.7 kcal mol^{-1}.

We have shown that the major difference between inhibitor A and B is the P1' substituent. It is thus reasonable to assume that the interaction energy between the enzyme and P1' substituent plays the most important role in the interaction energy decrement from complex A to complex B. To prove this assumption, we calculated the interaction energy of the two inhibitors' P1' substituents with the three residues described above (Asp-161, Glu-202, His-205). The results are shown in Table 11. From this we deduce that for the cases of Asp-161 and Glu-202, the change of the interaction energy of the P1' substituent between the three residues does make a great share of that of the inhibitor. However, the case of

Table 10 The electrostatic interaction energy between inhibitor and several important residue

	Asp-161 (kcal mol^{-1})	Glu-202 (kcal mol^{-1})	His-205 (kcal mol^{-1})
Inhibitor A	−1.27(0.92)	−22.29(2.35)	−26.66(0.81)
Inhibitor B	−4.01(0.85)	−30.20(1.90)	−28.37(0.89)
Delta	−2.74	−7.91	−1.71

Table 11 The electrostatic interaction energy between inhibitor's P1' substituent and several important residue

P1	Asp-161 (kcal mol^{-1})	Glu-202 (kcal mol^{-1})	His-205 (kcal mol^{-1})
A:$(CH_2)_3C_6H_{11}$	3.09(0.07)	5.96(0.48)	−1.08(0.04)
B:$(CH_2)_3C_6H_5$	0.38(0.09)	−0.12(0.30)	−0.02(0.02)
Delta	−2.71	−6.08	1.06

Table 12 The distance between the P1' substituent of inhibitors and Glu-202 and Asp-161

	P1' substituent to Glu-202(Å)	P1' substituent to Asp-161(Å)
Complex A	8.30	12.15
Complex B	6.04	10.05

Table 13 The component of the 1–4 electrostatic interaction energy between inhibitor and His-205

His-205	Inhibitor	Complex A (kcal mol^{-1})	Complex B (kcal mol^{-1})
NE2	HO1	−14.61(0.85)	−17.27(0.69)
NE2	N	12.15(0.29)	9.25(0.26)
NE2	C1	−19.27(0.27)	−17.94(0.49)
CE1	O1	0.67(0.01)	0.68(0.02)
CE1	O2	0.62(0.03)	0.78(0.03)
CD2	O1	5.91(0.09)	5.68(0.17)
CD2	O2	6.95(0.24)	6.77(0.36)

Table 14 The electrostatic interaction energy between inhibitor and His-205

	His205 (normal) (kcal mol^{-1})	His-205 (1–4) (kcal mol^{-1})
Inhibitor A	−20.34(0.80)	−6.32(0.51)
Inhibitor B	−18.89(1.08)	−9.48(0.89)
Delta	1.45	−3.16

His-205 is completely different. The electrostatic interaction energy difference for the P1' substituent is 1.06 kcal mol^{-1}, while for the inhibitor it is −1.71 kcal mol^{-1}.

First, we shall discuss the source of the electrostatic energy portion of the free energy for the case of Asp-161 and Glu-202. The case of His-205 will be discussed later, because it is concerned with the 1–4 electrostatic energy portion.

Both Asp-161 and Glu-202 were known as typical negatively charged residues, so the performance of an inhibitor can be predicted simply from the total charge of its P1' substituent. For inhibitor A, the total charge on the P1' substituent is −0.126|e|, while for inhibitor B it is −0.0074|e|. We measured the distance between the P1' substituent and the two residues, and the results are listed in Table 12. It is obvious that the distance between A and Glu-202 is larger than that between B and Glu-202. For the case of Asp-161, this distance is also larger for system A than for system B. This is because of Coulomb repulsion. We also note that the distance between P1 and Asp-161 is larger than between P1 and Glu-202. This is why the interaction between the inhibitor and Glu-202 is stronger than that between the inhibitor and Asp-161.

1–4 electrostatic interaction

Because we have placed a bond between His-205 and the catalytic zinc ion, there are large 1–4 electrostatic interactions between the enzyme and the inhibitor. We calculated the 1–4 electrostatic energy and the normal electrostatic interaction energy between the inhibitor and His-205, as illustrated in Table 12. We find that the 1–4 electrostatic energy of system A is 3.16 kcal mol^{-1} higher than that of system B. This also explains the 1–4 electrostatic interaction's contribution to the relative binding free energy, this positive contribution was observed in the "slow growth" approach.

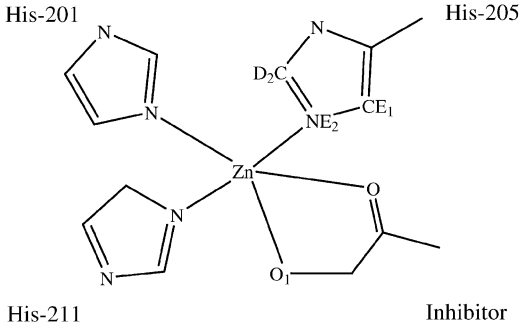

Scheme 1 The scheme of the binding site

There were seven pairs of atoms that had significant 1–4 electrostatic interactions. In order to gain a clear insight into which one is of the greatest importance, we calculated the electrostatic interaction energy in each pair of atoms. The results are shown in Table 13. To identify the atoms on the binding site, we assigned each atom a label, which can be seen in Scheme 1. It should be noted that the data listed here were not multiplied by the scale factor for the 1–4 electrostatic interactions (SCEE), which is 1.2 in our simulations, so the sum of the seven interaction energies is not equal to the total 1–4 electrostatic energies in Table 14. As can be seen, the first three atom pairs have larger differences than the others. These are NE2–HO1, NE2–N and NE2–C1. The partial charge of the four atoms (NE2, HO1, N and C) was same for the two complexes, so only the distance can affect the electrostatic energy. These distances are shown in Table 15.

We can now explain the transformation of the active site. Firstly, Glu-202 can form very strong hydrogen bonds with O1 and HO1 of the inhibitor, as mentioned in the Introduction. Secondly, the distance between His-205

Table 15 The distance between the atom pairs that have 1–4 electrostatic interactions

His-205	Inhibitor	Complex A (Å)	Complex B (Å)
NE2	HO1	2.85	2.52
NE2	N	3.80	3.73
NE2	C1	4.31	4.32

and inhibitor for complex A is larger than that for complex B5 because of the Coulomb repulsion between them. In complex A, Glu-202 is pushed away by the P1' substituent of inhibitor A, but the hydrogen bond between Glu-202 and HO1 is still maintained; HO1 is then pulled away from the atom NE2 of His-205 by the inhibitor. NE2 is negatively charged, while HO1 is positive, and increasing the distance between them causes the total energy of the complex system to increase. This is why complex A is less stable than complex B/MMP-2. This also explains the larger standard deviation of the distance and angle of the hydrogen bonds between Glu-202 and inhibitor A, which are shown in Table 3.

Structure comparison

After analyzing the interaction energy, we shall study the differences of two systems' structures. We calculated the averaged conformation of the MD trajectories of these two systems, and then fitted the two complex structures together. We found an RMS derivation between them of 1.49 Å. Moreover, after we extracted Asp-161, Glu-202, His-205 and the inhibitors from the two complexes and fitted again, the RMS derivation became 1.00 Å. This is consistent with the results of the energetic portion of our simulations.

Our discussions have shown that: (1) the P1' substituent of the inhibitor acts less well than that of inhibitor A in forming VDW interactions with the enzyme's S1 pocket; (2) only three residues behave differently between the two systems, and they are Asp-161, Glu-202 and His-205; (3) the behavior of the P1' substituent can represent that of the whole inhibitor for Asp-161 and Glu-202, and groups that have a positive electrostatic potential interact more favorably with the P1' substituent because of the negative electrostatic environment; (4) for His-205, the difference of 1–4 electrostatic interaction between the two system is the majority of the energy decrement, and this is the indirect influence of the inhibitors' P1' substituent.

These conclusions have been used to predict the binding affinity of other hydroxamate inhibitors. Inhibitor C, shown in Fig. 2, is very similar to inhibitor B. We have derived its RESP charges using the same procedure as for inhibitor B, and found that the total charge on its P1' substituent is –0.029|e|, which is lower than inhibitor B's –0.0074|e|, but much higher than inhibitor A's –0.126|e|. According to our conclusion, inhibitor C should perform much better than inhibitor B and worse than inhibitor A. The published experimental results support this conclusion. In the case of inhibitor D, the total charge on its P1' substituent is 0.0085|e|, which makes it a better inhibitor than inhibitor B, which is also supported by experiment. In the case of inhibitor E, the total charge on the P1' substituent is almost the same as for inhibitor B, so its binding affinity is almost the same as that of inhibitor B. All the data mentioned above are shown in Table 16.

Table 16 The total charge on inhibitors' P1' substituent and inhibitors' binding affinity

Inhibitor	Structure of P1' substituent	Total charge on P1' substituent	Ki (nM)
A	$-(CH_2)_3C_6H_{11}$	–0.126|e|	6.9
B	$-(CH_2)_3Ph$	–0.0074|e|	0.06
C	$-(CH_2)_3Ph$–4CF3	–0.029|e|	0.30
D	$-(CH_2)_3Ph$–4Cl	0.0085|e|	0.03
E	$-(CH_2)_3Ph$–4Me	–0.0039|e|	0.06

However, when we tried to extend the conclusion to a broader range of inhibitors, we found our prediction is not right at all. This is because we did not take van der Waals interaction into consideration in our model. For the case of inhibitors C, D and E, whose structures are very similar, this is not very important, but for the other inhibitors, their van der Waals interactions are totally different. This means our conclusion can be only used for structural modifications of inhibitor B.

Conclusions

We have obtained further insight into the role different inhibitor substituents play in protein–inhibitor interactions. Our simulations showed that all the necessary hydrogen bonds are satisfied and retained for both inhibitors.

The FEP simulations have shown that inhibitor B is more favorable than inhibitor A, but this effect relies on the electrostatic interaction, including normal and 1–4 electrostatic interactions. For the case of VDW interactions, inhibitor B is more favored than inhibitor A.

The residue of Glu-202 is of much greater importance than any other residue in the enzyme. It takes part in the catalytic process. Both inhibitors can form hydrogen bonds with Glu-202, but there are stronger electrostatic repulsions between inhibitor A and Glu-202 than between inhibitor B and Glu-202. This is the main reason why inhibitor B is more favorable, with electrostatic interactions with the inhibitor's zinc binding group and strong interactions with the inhibitor's P1' substituent.

We also found out that groups having a positive electrostatic potential were more preferred than those having a negative potential. The information could be useful for structural modification work based on inhibitor B.

Supplementary material

The inhibitors' and ions' RESP charges saved in AMBER lib format are supplied as supporting information.

Acknowledgment We would like to thank Dr. Linbo Zhang for his helpful advice in building the PC cluster. We are particularly grateful to the late Professor P.A. Kollman at UCSF for his distribution of AMBER 6.0 molecular simulation package and the newest AMBER force field parameters. This research was supported by the National Natural Science Foundation of China (NNSFC, No. 29992590-2).

References

1. Whittaker M, Floyd CD, Brown P, Gearing AJH (1999) Chem Rev 99:2735–2776
2. Buisson AC, Gilles C, Polette M, Zahm JM, Birembaut P, Tournier JM (1996) Lab Invest 74:658–669
3. Lafeur M, Underwood JL, Rappolee DA, Werb Z (1996) J Exp Med 184:2311–2326
4. Cawston TE (1996) Pharm Theor 70:163–182
5. Johnson LL, Dyer R, Hupe DJ (1998) Curr Opin Chem Biol 2:466–471
6. Massova I, Kotra LP, Fridman R, Mobashery S (1998) FASEB J 12:1075–1095
7. Liotta LA, Tryggvason K, Garbisa S, Robey PG, Abe S (1981) Biochemistry-US 20:100–104
8. Senior RM, Griffin GL, Fliszar CJ, Shapiro SD, Goldberg GI, Welgus HG (1991) J Biol Chem 266:7870–7875
9. Morgunova E, Tuuttila A, Bergmann U, Isupov M, Lindqvist Y, Schneider G, Tryggvason K (1999) Science 284:1667–1670
10. Lovejoy B, Hassell AM, Luther MA, Weigl D, Jordan SR (1994) Biochemistry 33:8207–8217
11. Bode W, Gomis-Ruth FX, Stocker W (1993) FEBS Lett 331:134–140
12. Chen LY, Rydel TJ, Dunaway CM, Pikul S, Dunham KM (1999) J Mol Biol 293:545–557
13. Hoops SC, Anderson KW, Merz KMJ (1991) J Am Chem Soc 113:8262–8270
14. Toba S, Damodaran KV, Merz KM (1999) J Med Chem 42:1225–1234
15. Hou TJ, Zhang W, Xu XJ (2001) J Phys Chem B 105:5304–5315
16. Hou TJ, Zhang W, Xu XJ (2002) J Comput Aid Mol Des 16:27–41
17. Zhang W, Hou TJ, Xu XJ (2001) Acta Chim Sinica 59:2116–2121
18. Hou TJ, Zhang W, Xu XJ (2001) Acta Chim Sinica 59:1184–1189
19. Vedani A, Huhta DW (1990) J Am Chem Soc 112:4759–4767
20. Stote RH, Karplus M (1995) Proteins 23:12–31
21. Hou TJ, Zhang, W, Xu XJ (2002) Acta Chim Sinica 60:221–227
22. Hou TJ, Guo SL, Xu XJ (2002) J Phys Chem B 106:5527–5535
23. Donini OAT, Kollman PA (2000) J Med Chem 43:4180–4188
24. Dhanaraj V, Williams MG, Ye QZ, Molina F, Johnson LL, Ortwine DF, Pavlovsky A, Rubin JR, Skeean RW, White AD, Humblet C, Hupe DJ, Blundell TL (1999) Croatica Chemica Acta 72:575–591
25. Poter JR, Beeley NRA, Boyce BA (1994) Bioorg Med Chem Lett 4:2741–2746
26. Insight II 95.0 User Guide (1995) Accelrys Inc, San Diego, Calif.
27. Frisch MJ, Trucks GW, Schlegel HB, Scuseria GE, Robb MA, Cheeseman JR, Zakrzewski VG, Montgomery JA, Stratman RE, Burant JC, Dapprich S, Millam JM, Daniels AD, Kudin KN, Strain MC, Farkas O, Tomasi J, Barone V, Cossi M, Cammi R, Mennucci B, Pomelli C, Adamo C, Clifford S, Ochterski J, Petersson GA, Ayala PY, Cui Q, Morokuma K, Malick DK, Rabuck AD, Raghavachari K, Foresman JB, Cioslowski J, Ortiz JV, Baboul AG, Stefanov BB, Liu C, Liashenko A, Piskorz P, Komaromi, I, Gomperts R, Martin RL, Fox DJ, Keith T, Al-Laham MA, Peng CY, Nanayakkara A, Gonzalez C, Challacombe M, Gill PMW, Johnson BG, Chen W, Wong MW, Andres JL, Gonzales C, Head-Gordon M, Replogle ES, Pople JA (1998) Gaussian 98. Gaussian, Pittsburgh, Pa.
28. Direct Force Field 1.0 User Guide (2001) Aeon Inc, San Diego, USA
29. Bayly CI, Cieplak P, Cornell WD, Kollman PA (1993) J Phys Chem 97:10269–10280
30. Cerius 2 User Guide (1995) Acceloys Inc, San Diego, USA
31. MOPAC 7.0 User Guide (1993) Quantum Chemistry Program Exchange (QCPE). Indiana University, USA
32. Case DA, Pearlman DA, Caldwell JW, Cheatham III TE, Ross WS, Simmerling CL, Darden TA, Merz KM, Stanton RV, Cheng AL, Vincent JJ, Crowley M, Tsui, V, Radmer RJ, Duan Y, Pitera J, Massova I, Seibel GL, Singh UC, Weiner P, Kollman PA (1999) AMBER 6.0. University of California, San Francisco, Calif.
33. Levy DE, Lapierre F, Liang W, Ye W, Lange CW, Li X, Grobelny D, Casabonne M, Tyrrell D, Holme K, Nadzan A, Galardy RE (1998) J Med Chem 41:199–223